

Data-driven methodologies for change detection in large-scale nonlinear dampers with noisy measurements

Hae-Bum Yun^{a,*}, Sami F. Masri^a, Raymond W. Wolfe^a, Gianmario Benzoni^b

^aViterbi School of Engineering, University of Southern California, Los Angeles, CA 90089-2531, USA

^bDepartment of Structural Engineering, University of California, San Diego, La Jolla, CA 92093-0085, USA

Received 4 December 2007; received in revised form 24 June 2008; accepted 6 November 2008

Handling Editor: S. Bolton

Available online 3 January 2009

Abstract

Large-scale viscous dampers are frequently used in civil structures to mitigate seismic and wind-induced vibration. For an effective condition assessment of nonlinear dampers, a probabilistic change detection methodology is proposed. The results of experimental studies with different large-scale nonlinear viscous dampers are shown. Considering damper experimental data with measurement uncertainty, the proposed data-driven methodology can be used to (1) detect small changes of a nonlinear system, (2) interpret the physical meanings of system changes, and (3) quantify the uncertainty of the detected changes without *a priori* knowledge of the system's characteristics.

© 2008 Elsevier Ltd. All rights reserved.

1. Introduction

1.1. Motivation

Large-scale orifice viscous dampers are frequently used in modern civil structures to mitigate seismic or wind-induced vibration. Among various types of dampers, orifice viscous dampers (hereinafter viscous dampers) provide excellent efficiency of energy dissipation—the orifice damper employs small orifices on its piston head, so that the silicon fluid sealed inside the damper chamber is forced to pass through the orifices when the damper piston reciprocates. Consequently, the dynamic properties of an orifice viscous damper largely depend on the geometric characteristics of the orifice design. Soong and Constantinou [1] and Soong and Dargush [2] provide detailed descriptions of orifice viscous dampers.

Due to their importance in applications involving civil structures, many government agencies require a series of quality assurance tests for large-scale dampers before the dampers are installed in actual civil structures [3–6]. After installation, the condition assessment of the installed dampers is commonly performed in two ways: visual inspection and monitoring the internal pressure of the damper's silicon fluid. First, visual inspection is usually conducted by trained inspectors, searching for noticeable damage on the damper surface,

*Corresponding author. Tel./fax: +1 213 740 6304.

E-mail address: haebum@usc.edu (H.-B. Yun).

Table 1

A comparison of investigated system identification methods for applications in structural health monitoring.

Identification methods	Advantages	Disadvantages
Simplified damper design model (parametric)	Most accurate if the exact system model is known Direct physical interpretation is possible using the identified parameters	<i>A priori</i> knowledge of the system is required The identified parameters become significantly biased when the initial model is incorrect
Restoring Force Method (non-parametric)	No <i>a priori</i> knowledge of the system is required The same model can be used when the system changes into different nonlinear classes It is applicable to a wide range of nonlinearities Both Chebyshev and power-series coefficients can be identified Physical interpretation of some of the identification results is possible with identified coefficients	The identification yields an approximating model Only limited physical interpretation of identification results is possible
Artificial neural networks (non-parametric)	No <i>a priori</i> knowledge of the system is required It is applicable to a wide range of nonlinearities Change detection of the system is possible through monitoring the regression error of the trained networks	Change detection is possible, but physical interpretation of the detected changes are not generally possible

often evident by fluid leakage. The second method employs a pressure gauge to measure the internal pressure levels of the dampers. Thus, with a pressure change, the inspectors can presume that the damper has changed during the operation. If the pressure change were significant, the damper would be removed from the structure and delivered to testing facilities to find possible causes of the change. However, none of the current practices are adequate for reliable condition assessment. The visual inspection is often subjective. Although the pressure monitoring is obviously a more advanced method than visual inspection, the direct relationships between the pressure level and engineering characteristics of the nonlinear dampers are difficult to identify. Moreover, no current practices of damper monitoring are appropriate when a number of dampers are employed in a structure. For example, after a major seismic retrofit of the west span of the San Francisco Oakland Bay Bridge in 2004, more than 100 large-scale viscous dampers are employed. In this case, more systematic and efficient condition assessment methodologies are required.

As an alternative approach for damper condition assessment, a vibration-based structural health monitoring technique is proposed in this study. Yun et al. [7] and Yun and Masri [8] demonstrated that the non-parametric Restoring Force Method is a very promising tool for the condition assessment of large-scale nonlinear viscous dampers. Comparing one parametric (the simplified damper design model) and two non-parametric identification methods (the Restoring Force Method and artificial neural networks), they demonstrated that the Restoring Force Method has significant advantages than other methods because (1) no *a priori* knowledge of the system is needed, (2) the same non-parametric model is applicable to a wide range of nonlinearities, and (3) the physical interpretation of the identification results is possible, which is generally impossible with other non-parametric identification methods, such as artificial neural networks. A comparison of three identification methods for structural health monitoring applications is shown in Table 1.

Recent progress in sensing and Internet-based data communication technologies allow the development of real-time remote monitoring systems for civil infrastructure system. Yun et al. [9] have developed a reliable real-time web-based continuous bridge monitoring system that has been applied to a critical bridge (the Vincent Thomas Bridge) in the Los Angeles, California, metropolitan region to perform forensic studies of various earthquakes, as well as a recent ship–bridge collision. Therefore, by combining the technology of a web-based monitoring system with the Restoring Force Method, a feasible

methodology can be developed for a real-time remote condition assessment of large-scale nonlinear viscous dampers.

In the development of the monitoring system, the following practical and challenging problems must be considered: First, the effects of measurement noise on the results of change detection must be considered, since sensor readings can be more significantly affected by noise in the *in situ* measurements than in laboratory testing, due to various sources of noise. In many cases of *in situ* monitoring, only the displacement or acceleration is measured, depending on the measurement feasibility, and then other necessary response states are numerically obtained through digital signal processing techniques using the measured response. In such cases, the effects of measurement noise are not simply additive, and propagate throughout the response states, which are numerically obtained from noisy measurements. Consequently, the developed methodology should be able to deal with those complicated noise effects. Second, the results of the change detection will be affected by the measurement uncertainty. Therefore, the uncertainty of the detected change due to the measurement noise must be quantified for reliable condition assessment. However, the uncertainty quantification requires multiple tests, which is not usually possible for the *in situ* monitoring due to lack of control of excitation sources. Even if one had the control of the excitation, performing multiple tests with full-scale viscous dampers is extremely difficult because of an enormous amount of heat converted from the dissipated energy.

Having the proposed condition assessment methodology will provide contributions in the following three ways:

1. Enabling the interpretation of physical significance of detected changes, one can quantify the significance of the changes at the full-structure level as well as at the component level. This attribute remains even when the dampers' evolving properties change into different classes of nonlinearity, due to various types of deterioration.
2. With more reliable condition assessment methodologies, one can minimize unnecessary removal of undamaged dampers. Damper removal from civil structures is time-consuming and expensive due to their large physical size.
3. Since the methodology proposed in this study is data-driven and model independent, the same approach is applicable to other types of nonlinear components, such as different types of energy dissipating devices, base isolators, and nonlinear joints.

1.2. Objective

The objective of this study is to develop a data-driven methodology for change detection in large-scale nonlinear viscous dampers. A joint study was performed between the University of Southern California, the University of California at San Diego and the University of California at Berkeley. Three different large-scale nonlinear viscous dampers were tested at the University of California at Berkeley and the University of California at San Diego. The damper experiments were designed to introduce different types of nonlinearity in a systematic way. Three large-scale viscous dampers used in the experimental study involved different nonlinear features. In the experiments, two different excitation types were tested, including monotonic sinusoidal and broadband random excitations.

Using the experimental results, an analytical study was performed at the University of Southern California. A data-driven change detection methodology for the tested large-scale dampers was investigated using the non-parametric Restoring Force Method. In order to study the effects of measurement uncertainty, the damper data were intentionally polluted with random noise. As a statistical data recycling technique, the Bootstrap method was investigated for uncertainty quantification, even with insufficient data for meaningful statistical inferences. Using the developed change detection methodology, the aim was to achieve the following:

1. ability to detect even small (genuine) changes in the nonlinear dampers;
2. ability to interpret the physical meaning of detected changes; and
3. ability to quantify the uncertainty associated with the detected changes.

1.3. Scope

This paper is organized as follows: the experimental studies using three large-scale nonlinear dampers are discussed in Section 2; the data-driven identification approach using the Restoring Force Method is discussed in Section 3; the uncertainty estimation and statistical change detection of the large-scale viscous dampers are discussed in Section 4; and the Bootstrap method as a data recycling technique and its uncertainty estimation are discussed in Section 5.

2. Experimental studies

2.1. Test apparatus

Three different large-scale nonlinear viscous dampers were tested at two different test facilities: the 66.7 kN (15 kip) viscous damper was tested at the Earthquake Engineering Research Center (EERC) of the University of California, Berkeley (Fig. 1(a)), and the 2001.6 kN (450 kip) and 2891.3 kN (650 kip) viscous dampers were tested at the Seismic Response Modification Device (SRMD) facility of the University of California, San Diego (Fig. 1(b)).

The 66.7 kN damper with the maximum velocity of 431.8 mm/s (Damper A) has the smallest size among the tested dampers in this study. The damper was designed using a simplified Maxwell model [10–14] as

$$r(x, \dot{x}) = C \operatorname{sgn}(\dot{x}) |\dot{x}|^n, \quad (1)$$

where r is the restoring force, C is the damping constant, and n is the nonlinear damping exponent. This simplified design model is valid when the excitation frequency is low. In this case, the inertia term of the damper response becomes insignificant, and consequently, $f(t) \approx r(x, \dot{x})$, where f is the measured force. Yun et al. [7] demonstrated that the inertia term of the large-scale damper response would be negligible at a low velocity. The design parameters of Damper A are $C = 1.12 \text{ kN s}^n/\text{cm}^n$ and $n = 1.0$, which makes the damper response approximately linear. The 2001.6 kN damper at the maximum velocity of 215.9 cm/s (Damper B) was designed with the parameters $C = 199.95 \text{ kN s}^n/\text{cm}^n$ and $n = 0.3$. The 2891.3 kN damper at the maximum velocity of 40.6 cm/s (Damper C) was designed with $C = 957.44 \text{ kN s}^n/\text{cm}^n$ and $n = 0.3$. Hence, the restoring force of Dampers B and C will be “softening” with $n < 1.0$.

2.2. Test protocols and preliminary data processing

2.2.1. Test with Damper A

Damper A was subjected to broadband random excitation with a lowpass cutoff frequency of 5.0 Hz. During the experiment, the acceleration (\ddot{x}) and force (f) of the damper were measured with a sampling

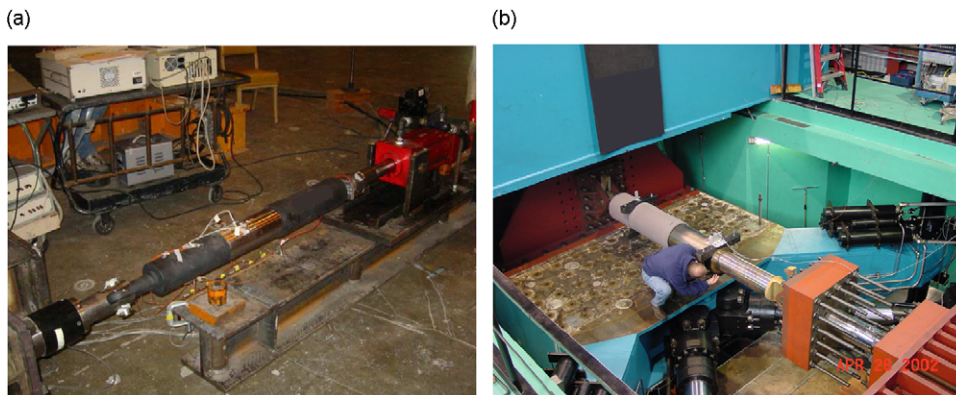


Fig. 1. Test facilities for large-scale viscous dampers at the University of California, Berkeley (UCB), and the University of California, San Diego (UCSD) used in this study. (a) Test at the University of California, Berkeley. (b) Test at the University of California, San Diego.

frequency of 1 kHz. The measured force of Damper A under broadband random excitation is shown in Fig. 2(a). Once \ddot{x} and f were measured, preliminary data processing was performed to obtain the displacement (x) and velocity (\dot{x}) required for the damper identification. The data processing was performed in accordance with the following procedures:

1. The measured \ddot{x} and f were de-trended and zero-phase filtered with the cutoff frequencies of 0.1–10.0 Hz, and a cosine-tapered window was applied to the time histories of \ddot{x} and r .
2. The filtered \ddot{x} was integrated to obtain the corresponding velocity \dot{x} . The same filter and time-history window were applied to \dot{x} .
3. The processed \dot{x} was numerically integrated to obtain the corresponding displacement x . The same filter and time-history window were also applied to x .

The test protocols, preliminary data processing and phase plots of the resulting Damper A response are summarized in Table 2.

2.2.2. Test with Dampers B and C

Dampers B and C were subjected to monotonic sinusoidal excitation with an excitation frequency of 0.2 Hz for both dampers. Unlike Damper A, x and f (but not the \ddot{x}) were measured during the experiments. The sampling frequency of the measurement was 100 Hz. Fig. 2(b) and (c) show the measured force of Dampers B and C, respectively. In the figures, notice that the force amplitude of Damper B is constant, while that of

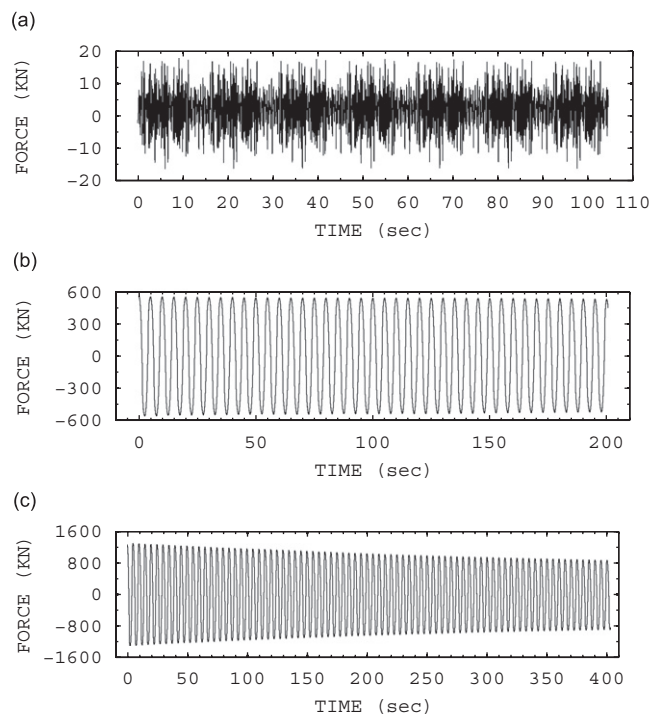
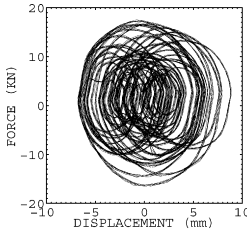
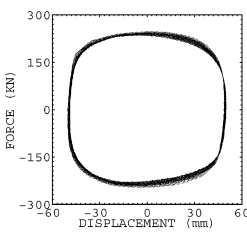
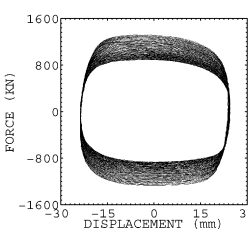
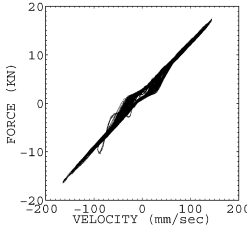
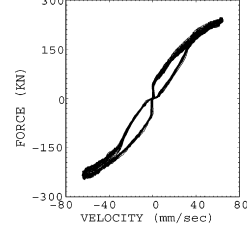
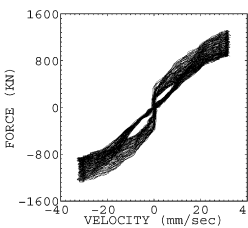


Fig. 2. Time histories of the measured forces for different large-scale nonlinear viscous dampers with displacement-controlled excitations. (a) The force of Damper A was measured under broadband random excitation. Damper A was a time-invariant system whose characteristic was close to linear. (b) The force of Damper B was measured under monotonic sinusoidal excitation with a constant frequency of 0.2 Hz and constant peak amplitudes of ± 50.8 mm. The measured time history shows that Damper B is a time-invariant system. The damping response of Damper B was hysteretic with damping “softening”. (c) The force of Damper C was measured under monotonic sinusoidal excitation with a constant frequency of 0.2 Hz and constant peak amplitudes of ± 25.4 mm. Damper C was a time-varying system, since the measured force decreases with the constant monotonic sinusoidal excitation, while Dampers A and B are time-invariant systems. Similar to Damper B, the damping response of Damper C was hysteretic with damping “softening”.

Table 2

Summary of test protocols and preliminary data processing parameters for the three large-scale nonlinear viscous dampers used in this study.

Parameters	Damper A	Damper B	Damper C
Nominal output force kN (kips)	66.7 (15)	2001.6 (450)	2891.3 (650)
Max. velocity rating cm/s (ips)	43.2 (17)	215.9 (85)	40.6 (16)
Designed parameters for damping, $kN (s/cm)^n$	$C = 1.12, n = 1.0$	$C = 398.93, n = 0.3$	$C = 957.44, n = 0.3$
Excitation type	Broadband random	Monotonic sinusoidal	Monotonic sinusoidal
Excitation frequency (Hz)	≤ 5.0	0.2	0.2
Nonlinearity	Close to linear	Polynomial, hysteretic	Polynomial, hysteretic
Time-invariancy	Time-invariant	Time-invariant	Time-varying
Measured response	\ddot{x}, f	x, f	x, f
Performed data processing	Integration for \dot{x} Double integration for x	Differentiation for \dot{x}	Differentiation for \dot{x}
Stiffness response			
Damping response			

Damper C decreases. Both dampers were subjected to the sinusoidal excitation with a constant frequency and constant peak amplitudes over time.

Once x and f are measured for Dampers B and C, preliminary data processing was performed to obtain the velocity (\dot{x}) using the following procedures:

1. The measured x and f were de-trended and zero-phase filtered with the cutoff frequencies of 0.05–5.0 Hz. Then, a cosine-tapered window was applied to the time histories of the filtered response, x and f .
2. The displacement x was differentiated to obtain the corresponding \dot{x} . The same filter and time-history window were applied to the obtained \dot{x} .

The test protocols, preliminary data processing and phase plots of Dampers B and C are summarized in Table 2.

3. Non-parametric identification

3.1. Overview of Restoring Force Method

The Restoring Force Method is a non-parametric identification method for nonlinear systems, using a series expansion of two-dimensional Chebyshev polynomials [15]. Using the Restoring Force Method, the restoring

force of a single-degree-of-freedom (sdf) nonlinear dynamic system can be modeled as

$$r(x, \dot{x}) = \sum_{i=0}^P \sum_{j=0}^Q \bar{C}_{ij} T_i(\bar{x}) T_j(\bar{\dot{x}}), \quad (2)$$

where $r(x, \dot{x})$ is the restoring force of the nonlinear dynamic system, \bar{C}_{ij} is the normalized Chebyshev coefficient, $T_i(\bullet)$ is the i th-order Chebyshev polynomial, P and Q are the highest orders of the Chebyshev polynomial of the normalized displacement (\bar{x}) and velocity ($\bar{\dot{x}}$), respectively, within the range of $[-1, 1]$.

Once the \bar{C}_{ij} are identified, the \bar{C}_{ij} can be converted into the equivalent power-series coefficients using the following relationship [16]:

$$T_0(y) = 1, \quad T_1(y) = y, \quad T_2(y) = 2y^2 - 1, \dots, \quad T_{k+1}(y) = 2yT_k(y) - T_{k-1}(y), \dots \quad (3)$$

The converted power-series coefficients are called the normalized power-series coefficients (\bar{a}_{ij}). With the de-normalization of \bar{x} and $\bar{\dot{x}}$, the de-normalized power-series coefficients (a_{ij}) can be obtained. Using these coefficients, Eq. (2) can be also expressed as

$$r(x, \dot{x}) = \sum_{i=0}^P \sum_{j=0}^Q \bar{C}_{ij} T_i(\bar{x}) T_j(\bar{\dot{x}}) = \sum_{i=0}^P \sum_{j=0}^Q \bar{a}_{ij} \bar{x}^i \bar{\dot{x}}^j = \sum_{i=0}^P \sum_{j=0}^Q a_{ij} x^i \dot{x}^j. \quad (4)$$

Accurate force measurement is critical for successful RFM applications. With the installation of load cells at the ends of sdf viscous dampers, it can be conducted relatively easily to measure the force time histories. Since there are various types of load cells available with long-term stability and robustness, reliable force measurements is relatively easy to achieve.

3.2. Identification of nonlinear viscous dampers

It was known that the force characteristics for Dampers A and B do not change over time under stationary displacement-controlled excitation. For example, as shown in Fig. 2(b), the measured force of Damper B is *stationary* over time under the *stationary* sinusoidal excitation with a constant frequency of 0.2 Hz and constant peak amplitudes of ± 50.8 mm. Consequently, since the outputs (i.e., measured force) of Dampers A and B do not depend explicitly on time, the dampers are *time-invariant systems* under *stationary* excitation. On the other hand, as shown in Fig. 2(c), the measured force of Damper C decreases over time although the sinusoidal excitation has a constant frequency of 0.2 Hz and constant peak amplitudes of ± 25.4 mm. Hence, Damper C is a *time-varying system* since the output of Damper C depends on time under *stationary* excitation. For these two classes of nonlinear systems (time-invariant and time-varying), different procedures were applied in the damper identification. Detailed identification procedures for each class are described below.

3.2.1. Identification results of time-invariant systems

Using the *time-invariant* systems of Dampers A and B, the Restoring Force Method identification was applied for the entire domain of the measured time histories. In both cases, the order of the series expansion was five. The identification results for Dampers A and B are shown in Fig. 3. The quality of the Restoring Force Method identification was measured with the normalized mean-square errors (NMSE) as

$$\text{NMSE} = \frac{1}{n\sigma_f^2} \sum_{i=1}^n (f_i - \hat{f}_i)^2, \quad (5)$$

where n is the number of data points, f is the measured force, \hat{f} is the identified force, and σ_f is the standard deviation of the measured force [17]. Considering Damper A, excellent identification results were obtained with the NMSE of 0.82% as illustrated in Fig. 3(a). For Damper B, “softening” hysteresis were successfully identified (Fig. 3(b)). However, the identification failed to accurately model the nonlinearity near the damper’s neutral position (i.e., $x \approx 0$ and $\dot{x} \approx 0$). The NMSE for the Damper B identification was 3.0%.

The identified Restoring Force Method coefficients for Dampers A and B are summarized in Table 3. For the normalized Chebyshev coefficients (\bar{C}_{ij}), the first-order damping coefficient (\bar{C}_{01}) is dominant for both

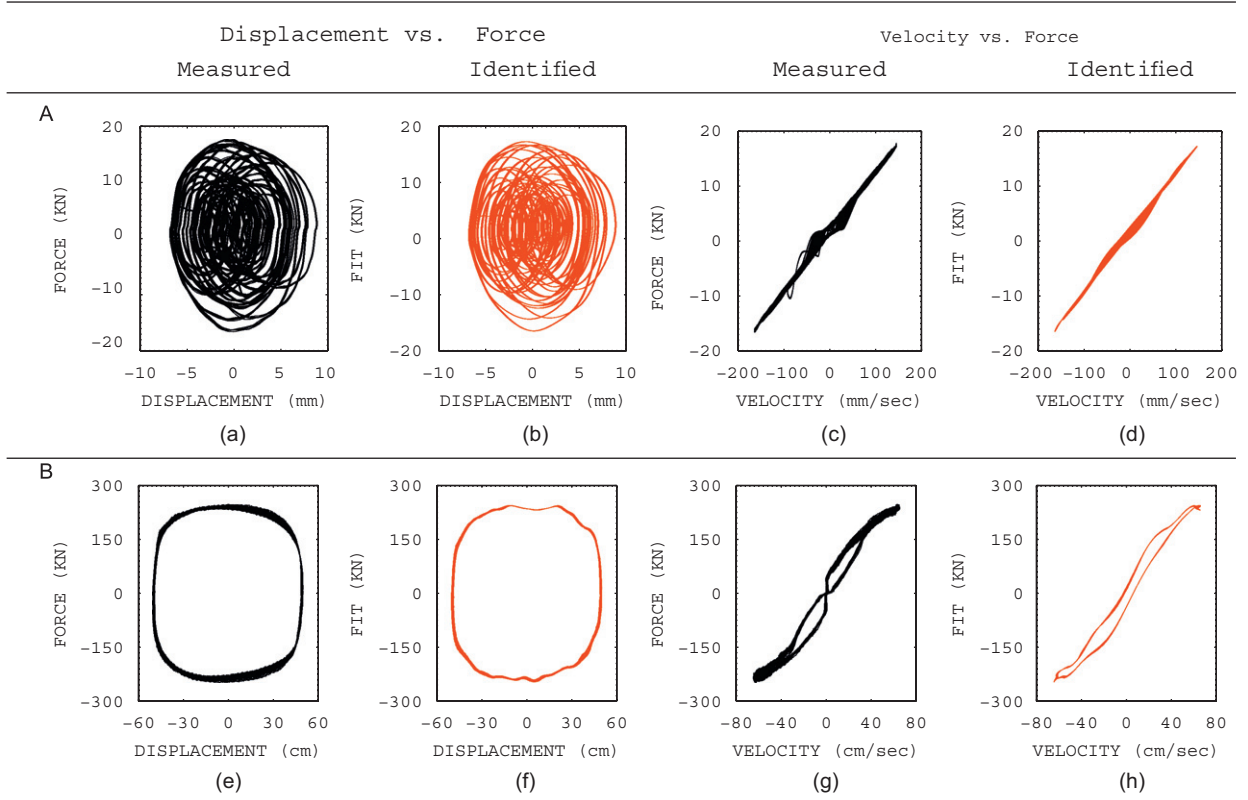


Fig. 3. The identification results for Dampers A and B using the Restoring Force Method.

Dampers A and B: 27.99 for Damper A and 257.00 for Damper B. Notice that Damper B is designed for a larger damping capacity than Damper A (refer Table 2). The third-order damping coefficient of Damper B ($\bar{C}_{03} = -13.17$) is negative because the designed damping exponent is less than one ($n = 0.3$), while the \bar{C}_{03} of Damper A is close to zero ($\bar{C}_{03} = 0.30$) because Damper A was designed for $n = 1.0$ (Eq. (1)). The stiffness-related coefficients (\bar{C}_{10} for the linear stiffness and \bar{C}_{30} for the cubic stiffness) are relatively small compared to the damping coefficient (\bar{C}_{01}) for both dampers, which indicates that the contribution of the stiffness terms is less significant in the identification than the damping terms (i.e., \bar{C}_{01} and \bar{C}_{03}). These results are reasonable for viscous dampers.

The identified power-series coefficients (\bar{a}_{ij} and a_{ij}) also show the damper nonlinearity without *a priori* knowledge of the dampers. For Damper A, the cubic damping coefficient ($\bar{a}_{03} = 4.21$) is ignorable, compared to the linear damping ($\bar{a}_{01} = 25.82$). This result indicates that the damping characteristic of Damper A is closed to linear rather than “softening”. On the other hand, the significance of the cubic damping coefficient ($\bar{a}_{03} = 148.20$) with respect to the linear damping coefficient ($\bar{a}_{01} = 203.10$) becomes larger for Damper B. However, since the \bar{a}_{03} is still smaller than the \bar{a}_{01} , the force of Damper B is “softening”. The identified Restoring Force Method coefficients for Dampers A and B are summarized in Table 3.

3.2.2. Identification results of time-varying system

In order to identify a *time-varying* nonlinear system of Damper C, the time histories of the damper data (i.e., x , \dot{x} and f) were partitioned into eight windows as illustrated in Fig. 4. The time-history partition was designed to have 10 cycles per window.

Then, the Restoring Force Method identification was performed for each time-history window. Damper C was accurately identified, and the mean and standard deviation of the NMSE for the eight windows were 0.50% and 0.09%, respectively. The identified normalized Chebyshev coefficients and normalized power-series

Table 3
Summary of the identified coefficients using the Restoring Force Method.

Coefficients	Damper A	Damper B	Damper C						
			(Parsed domain)						(Entire domain)
			Mean	Stdv	Max	Min			
\hat{C}_{10}	1.24E-2	40.27	37.59	21.01	55.79	-1.48	51.27		
\hat{C}_{01}	27.99	257.00	516.48	64.64	625.80	436.66	526.6		
\hat{C}_{30}	0.63	2.80	3.75	2.06	7.04	0.98	10.90		
\hat{C}_{03}	0.30	-13.17	-26.70	3.47	-21.67	-30.63	-52.09		
\hat{a}_{10}	-1.41	66.32	31.02	56.63	100.30	-59.67	72.60		
\hat{a}_{01}	25.82	203.10	430.40	41.33	490.90	373.30	507.9		
\hat{a}_{30}	-0.55	10.33	101.20	48.11	155.90	38.70	17.38		
\hat{a}_{03}	4.21	148.20	244.66	115.71	387.80	89.29	117.0		
\hat{a}_{10}	-0.19	1.33	1.33	2.37	4.18	-2.47	3.02		
\hat{a}_{01}	0.27	3.12	13.17	1.24	14.92	11.38	15.37		
\hat{a}_{30}	2.11E-5	7.38E-5	7.08E-3	3.38E-3	1.08E-2	2.90E-3	1.37E-3		
\hat{a}_{03}	3.68E-6	5.34E-4	6.94E-3	3.37E-3	1.08E-2	2.35E-3	3.04E-3		
NMSE (%)	0.82	5.03	0.50	0.09	0.66	0.39	1.92		

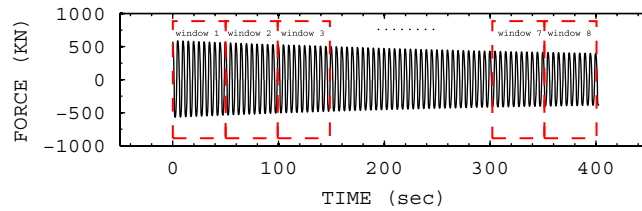


Fig. 4. Partitioning the time history of the measured force of Damper C for the Restoring Force Method identification.

coefficients for the eight windows are illustrated in Fig. 5. For the normalized Chebyshev coefficients (\hat{C}_{ij}), the linear damping (\hat{C}_{01}) is dominant with the mean value of 516.48, while the cubic stiffness (\hat{C}_{30}) is negligible with the mean value of 3.75. The linear damping coefficient (\hat{C}_{01}) decreases as the measured force decreases (Fig. 5(b)), while the linear stiffness (\hat{C}_{10}) remains constant (Fig. 5(a)). The cubic damping coefficient (\hat{C}_{03}) decreases as the damper reciprocates. For the normalized power-series coefficients (\hat{a}_{ij}), the first-order damping (\hat{a}_{01}) and third-order damping (\hat{a}_{03}) decrease (Fig. 5(f) and (h)), while the first-order stiffness (\hat{a}_{10}) and third-order stiffness remain constant (Fig. 5(e) and (g)). These results indicate that the degrading force of Damper C is due to the change of damping characteristics rather than stiffness characteristics over time.

The identified Restoring Force Method coefficients for Damper C are summarized in Table 3. In the table, the mean, standard deviation, maximum and minimum values of the Restoring Force Method coefficients identified for the eight identification windows in Fig. 4 are shown. For a comparison purpose, Damper C was also identified using the entire domain of measured time histories, and the corresponding identified Restoring Force Method coefficients for the entire time domain are also shown in the last column of Table 3. The table shows that the dominant coefficients for the entire time-history data are within the range of the minimum and maximum for the partitioned time-history data (e.g., $-1.48 \leq 51.27 \leq 55.79$ for the \hat{C}_{10} and $436.66 \leq 526.60 \leq 625.80$). The NMSE of the former is also about 3.5 times greater than the latter. The measured and identified forces using the entire time domain are compared in

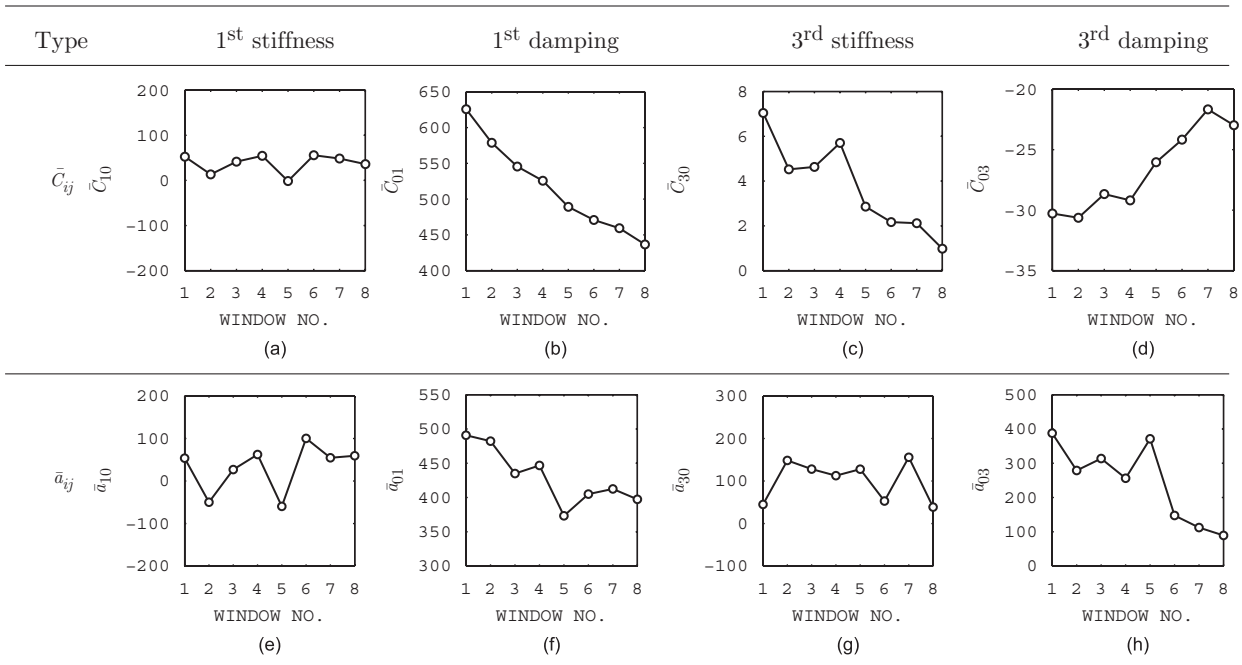


Fig. 5. The identified coefficients of Damper C for different time-history windows. (a)–(d) are the identified coefficients for different windows of the first-order stiffness, first-order damping, third-order stiffness and third-order damping terms, respectively, for the normalized Chebyshev coefficients (\bar{C}_{ij}). (e)–(h) are the same terms for the normalized power-series coefficients (\bar{a}_{ij}).

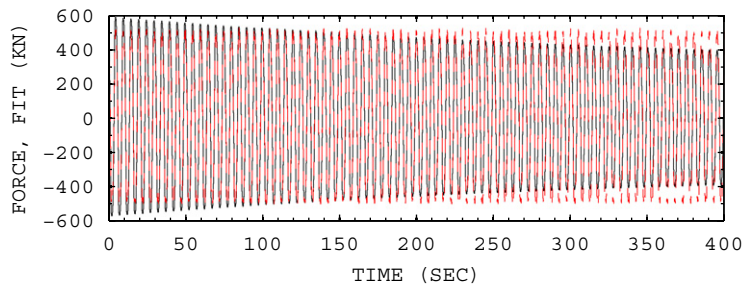


Fig. 6. The measured and identified forces for the time-varying system of Damper C under the stationary sinusoidal excitation with a constant frequency of 0.2 Hz and constant peak displacements of ± 25.4 mm using the entire domain of measured time histories of displacement, velocity and force. In the figure, the measured force is in the solid line, and the identified force is in the dashed line.

Fig. 6. The figure illustrates that the identified force estimates the average of the degrading measured force over time.

3.2.3. Findings from the identification results

Based on above results, several important conclusions can be drawn. First, two different types of nonlinear dampers were accurately identified without using a priori knowledge about the identified dampers. This is because the identification procedures of the Restoring Force Method are data-driven and model-independent. Although no *a priori* knowledge was used in the identification, the identified Chebyshev and power-series coefficients still contain the information concerning the dominant physical characteristics of the identified dampers. Consequently, in the development of the change detection methodology, these coefficients can be used as “change indicators” (or “features” in pattern recognition sense). Moreover, knowing which

coefficients the changes were observed in, one can interpret the physical meanings of the detected changes. Hence, guidelines to deal with the detected changes can be established for field applications. An excellent example can be found in the identification results of Damper C. Again, without a priori knowledge of the time-varying damper, the identified coefficients show that the decreasing measured force is due to degradation of the damping efficiency (decreasing damping coefficients) in time rather than the changes of damper stiffness (constant stiffness coefficients).

Notice that although the identified normalized Chebyshev coefficients (\bar{C}_{ij}) are related to the dampers' stiffness or damping characteristics, they are not exactly equivalent to the actual spring or damping constants of the dampers. For physical interpretation purposes, the normalized power-series coefficients (\bar{a}_{ij}) and denormalized power-series coefficients (a_{ij}) can be used as more convenient indices. However, the \bar{C}_{ij} have many advantages over \bar{a}_{ij} and a_{ij} , because of the orthogonal property of the Chebyshev polynomials. The orthogonal property of \bar{C}_{ij} can reduce the complexity of the uncertainty quantification of change detection with noisy measurements. Detailed discussion of this issue is provided in Section 4.3.

4. Uncertainty estimation of damper identification

4.1. Data generation of noisy response

In order to study the effects of measurement noise on the damper identification, the sensor measurements of Dampers A–C were polluted with 5% additive zero-mean Gaussian noise with respect to the root-mean-square (rms) of the measurement states: the acceleration (\ddot{x}) and force (f) for Damper A, and the displacement (x) and force (f) for Dampers B and C. Once the measurement states were polluted, the necessary damper response for the Restoring Force Method identification was obtained numerically with the noisy measurements: x and \dot{x} for Damper A, and \dot{x} for Dampers B and C. Hence, the uncertainty of the noisy measurements propagated throughout the numerically obtained response. The detailed data processing procedures were the same as those described in Section 2.2. A total of 3000 noisy data sets were generated for all tested dampers. Sample time histories of noisy data sets for Damper B are shown in Fig. 7.

4.2. Damper identification with noisy response

Once the 3000 noisy data sets were obtained for each damper, the Restoring Force Method identification was performed, and the corresponding Chebyshev coefficients (\bar{C}_{ij}) and power-series coefficients (\bar{a}_{ij} and a_{ij}) were identified. The NMSE of the Restoring Force Method identification was relatively low for all tested

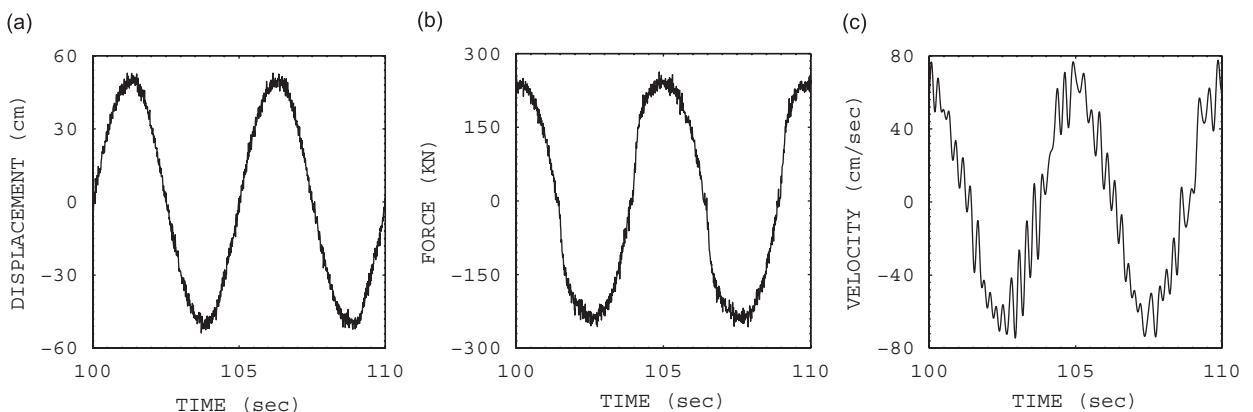


Fig. 7. Sample time histories of noisy response of Damper B. (a) and (b) The measured displacement and force polluted with 5% zero-mean additive Gaussian random noise. (c) The velocity obtained through the numerical differentiation of the polluted displacement using the data processing procedures discussed in Section 2.2. Consequently, the effects of noise in the obtained velocity is more complicated than the simple additive Gaussian noise in the noisy displacement and force.

dampers: the mean and standard deviation of the NMSE for Damper A were 1.33% and 0.79%, respectively; those for Damper B were 3.91% and 2.54%, respectively; and those for Damper C were 4.59% and 2.98%, respectively.

For the linear damping (\bar{C}_{01}), which was the dominant term in the identification, the mean of \bar{C}_{01} for Damper A was 16.84, which was 61.16% compared to the identified \bar{C}_{01} of 27.99 using the “clean” data set, while the means of \bar{C}_{01} for Dampers B and C were 278.06 and 562.48, respectively, which were 108.19% and 108.91%, compared to the identified \bar{C}_{01} of 257.00 and 516.48, respectively, using the “clean” data set. Hence, the discrepancy between the identified \bar{C}_{01} for “clean” and “noisy” data was larger with Damper A than with Dampers B and C.

The statistics of identified coefficients for Dampers A–C using the Restoring Force Method are summarized in Table 4. The table shows that the coefficients of variance (cv) of \bar{C}_{01} and the cubic damping (\bar{C}_{03}) for Dampers B and C are almost identical: the cv of \bar{C}_{01} for Dampers B and C were 0.03 and 0.03, respectively, and the cv of \bar{C}_{03} were -0.15 and -0.18 , respectively. This result is expected since the “softening” characteristics of Dampers B and C are similar with the same designed damping exponent ($n = 0.3$). On the other hand, Damper A has a different cv (cv of $\bar{C}_{03} = -5.00$) because the designed damping exponent for Damper A was $n = 1.0$. Hence, physical interpretation using the identified coefficient was still valid even with the noisy measurements.

The uncertainty levels of the identified Chebyshev and power-series coefficients are not necessarily linear with the levels of measurement uncertainty. For example, as shown in Table 4, the standard deviation of \bar{C}_{01} for Damper B is 14.26 with 5% rms of zero-mean Gaussian noise in the displacement and force, and the velocity obtained with the numerical differentiation of the noisy displacement. If the rms noise level increases to 10%, the standard deviation of \bar{C}_{01} is expected to increase, but not necessarily become 28.52 (i.e., double of the original value). The relationship between the measurements noise level and

Table 4
Statistics of the identified Restoring Force Method coefficients for the multiple tests and 3000 noisy data sets.

Type	Damper A			Damper B			Damper C ^a		
	Mean	Stdv	cv	Mean	Stdv	cv	Mean	Stdv	cv
(a) Normalized Chebyshev coefficients (\hat{C}_{ij})									
\hat{C}_{10}	0.67	0.19	0.28	26.23	14.26	0.54	55.19	32.17	0.58
\hat{C}_{01}	16.84	0.16	0.01	278.06	8.60	0.03	562.48	17.17	0.03
\hat{C}_{30}	0.14	0.14	1.00	-6.05	14.09	-2.33	-6.17	28.40	-4.60
\hat{C}_{03}	-0.02	0.10	-5.00	-62.46	9.14	-0.15	-112.19	20.71	-0.18
(b) Normalized power-series coefficients (\hat{a}_{ij})									
\hat{a}_{10}	1.55	0.69	0.45	110.49	115.28	1.04	286.46	245.46	0.86
\hat{a}_{01}	18.23	0.74	0.04	642.43	86.03	0.13	1093.50	198.68	0.18
\hat{a}_{30}	-1.20	2.32	-1.93	-190.07	360.35	-1.90	-473.24	786.05	-1.66
\hat{a}_{03}	-2.63	2.26	-0.86	-747.97	322.88	-0.43	-982.85	669.23	-0.68
(c) De-normalized power-series coefficients (\hat{a}_{ij})									
\hat{a}_{10}	1.42E-1	6.27E-2	0.44	2.00	2.09	1.05	10.98	7.85	0.71
\hat{a}_{01}	1.17E-1	5.56E-3	0.05	7.25	0.90	0.12	26.25	3.63	0.14
\hat{a}_{30}	-6.04E-4	2.36E-3	-3.91	-1.10E-3	2.12E-3	-1.93	-2.56E-2	4.24E-2	-1.66
\hat{a}_{03}	-8.17E-7	6.69E-7	-0.82	-1.05E-3	4.35E-4	-0.41	-1.31E-2	8.32E-3	-0.64
(d) Normalized root-mean-square of identification errors									
NMSE	1.33E-2	7.90E-3	0.59	3.91E-2	2.54E-2	0.65	4.59E-2	2.98E-2	0.65

The mean, standard deviation and coefficient of variation are shown. In this table, only significant coefficients are shown, including the linear stiffness (\bar{C}_{10} , \bar{a}_{10} , a_{10}), linear damping (\bar{C}_{01} , \bar{a}_{01} , a_{01}), cubic stiffness (\bar{C}_{30} , \bar{a}_{30} , a_{30}), and cubic damping (\bar{C}_{03} , \bar{a}_{03} , a_{03}).

^aThe coefficients of Damper C are the averaged values for eight time-history windows shown in Fig. 4.

uncertainty levels of the identified coefficients is a complex nonlinear function, affected by the type of dynamic systems, stochastic characteristics of measurements uncertainty, and orthogonality of the identified coefficients.

4.3. Statistical change detection of time-varying damper

4.3.1. Statistical independence of the Restoring Force Method coefficients

In Section 3.2, it was shown that the identified Restoring Force Method coefficients can be used as excellent “change indicators”. A question is left: among three kinds of Restoring Force Method coefficients, which one is most useful for change detection in a *probabilistic* sense. The advantage of using the de-normalized power-series coefficients (a_{ij}) is that direct physical interpretation is possible because the a_{ij} preserves the physical units (e.g., the unit of a_{10} for Damper B is kN/mm, that is the same as the linear spring constant). The advantage of using the normalized power-series coefficients (\bar{a}_{ij}) is that although the direct physical interpretation is not convenient due to using the normalized displacement (\bar{x}) and velocity ($\dot{\bar{x}}$), \bar{a}_{ij} measures the relative contribution of each power-series term to the identified restoring force. However, when measurement uncertainty exists, the identified a_{ij} and \bar{a}_{ij} are not statistically independent because the basis functions of the power-series expansion (i.e., $x^i \dot{x}^j$ and $\bar{x}^i \dot{\bar{x}}^j$) are not orthogonal. Consequently, for the uncertainty quantification of the system changes, the testing dimension of the statistical Hypothesis Test becomes too high because the a_{ij} and \bar{a}_{ij} are multivariate coefficients. For example, in this study, there are 36 identified coefficients with the highest series order of five for the displacement and velocity. For a_{ij} and \bar{a}_{ij} , because each of the coefficients are not statistically independent, the Hypothesis Test should be performed with the testing dimension of 36 (maximum). In Fig. 8(a), the scatter plot between the first-order damping (\bar{a}_{01}) and linear stiffness (\bar{a}_{10}) shows no significant statistical correlation. However, a strong correlation is observed between the linear damping (\bar{a}_{01}) and cubic damping (\bar{a}_{03}).

On the other hand, the normalized Chebyshev coefficients (\bar{C}_{ij}) preserves the *statistical independence* because the basis function of Chebyshev polynomials are *orthonormal* [16]. In Fig. 8(b), both scatter plots illustrate that no significant statistical correlations are observed between the identified Chebyshev coefficients. With the statistical independence property, the testing dimension of the Hypothesis Test dramatically reduces to *one*. That is, the Hypothesis Test can be performed for each individual Chebyshev coefficient to detect possible system changes. Hence, the normalized Chebyshev coefficients were used in the statistical change detection in this study.

4.4. Statistical change detection using identified coefficients

Using the 3000 sets of the identified, normalized Chebyshev coefficients (\bar{C}_{ij}), the distributions of the identified \bar{C}_{ij} were obtained. The histograms of the identified first-order damping coefficient (\bar{C}_{01}), the dominant coefficient in the Damper C identification, for different time-history windows are shown in Fig. 9. The bin width of the histograms was determined using the normal reference rule (or Scott’s rule) [18,19], optimized for the Gaussian distribution as

$$h = 3.5S_x N^{-1/3}, \quad (6)$$

where h is the bin width (or smoothing factor), S_x is the sample standard deviation of a statistic of interest X , and N is the sample size. The probability density functions (pdf) of \bar{C}_{01} were estimated with the Gaussian distribution assumption and are shown in Fig. 9. In the figure, the mean of the distributions decrease in time, while the standard deviations of the distributions remain approximately constant. The pseudo-constant deviation is the justification as to why the noise amplitudes were fixed at 5% rms with respect to the measurement states among the windows (Section 4.1). After obtaining the distributions of identified coefficients, one can achieve the three objectives of this study that were discussed in Section 1.2. First, with the mean of the distribution, one can accurately check if the damper has had a genuine system change. Second, one can interpret the physical meaning of the detected changes. In Sections 3.2 and 4.2, it was shown that the actual changes in Damper C are due to the degradation of the damping efficiency rather than stiffness efficiency. Third, with the standard deviations of the distributions determined, one can quantify the

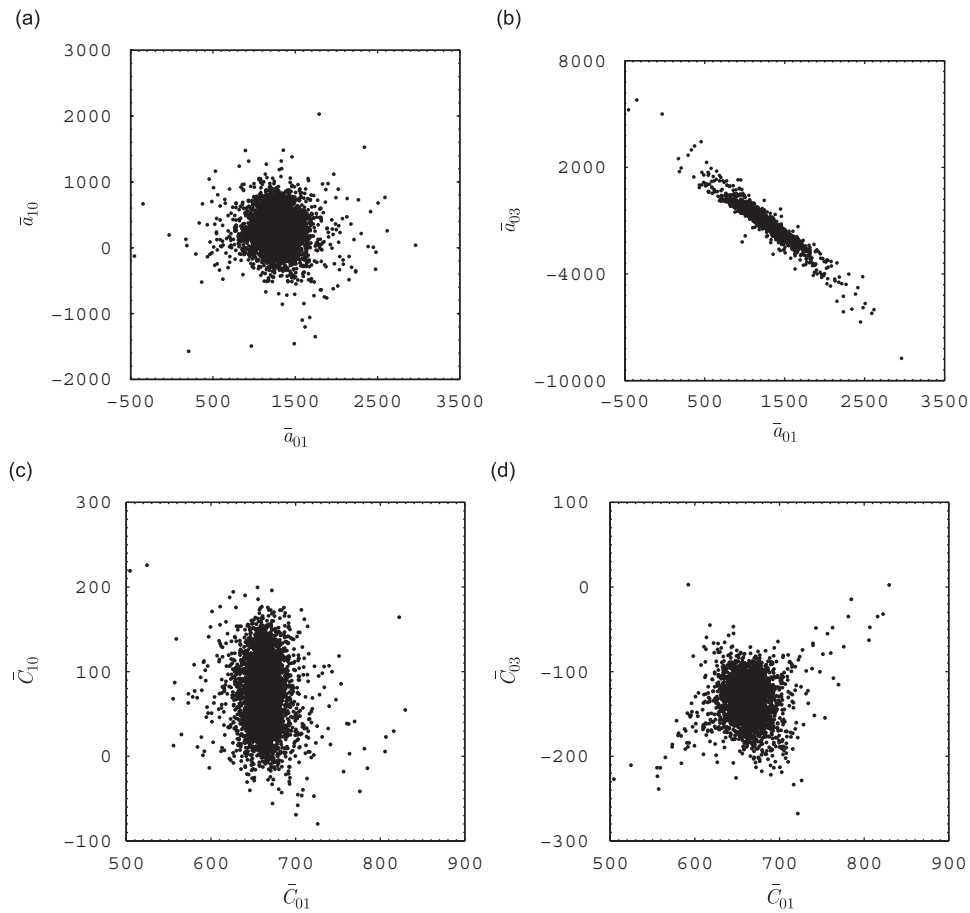


Fig. 8. Sample scatter plots of the normalized power-series coefficients (\bar{a}_{ij}) and normalized Chebyshev coefficients (\bar{C}_{ij}) for the noisy response of Damper C (Window 1 in Fig. 4) and their coefficients of variance (ρ). The magnitude of the linear correlation coefficient (ρ) between two identified coefficients is also shown in the table. (a) is of the normalized power-series coefficients between the first-order damping (\bar{a}_{01}) and first-order stiffness (\bar{a}_{10}). $\rho(\bar{a}_{01}, \bar{a}_{10}) = -0.04$. (b) is of the normalized power-series coefficients between the first-order damping (\bar{a}_{01}) and third-order damping (\bar{a}_{03}). $\rho(\bar{a}_{01}, \bar{a}_{03}) = -0.96$. (c) is of the normalized Chebyshev coefficients between the first-order damping (\bar{C}_{01}) and first-order stiffness (\bar{C}_{10}). $\rho(\bar{C}_{01}, \bar{C}_{10}) = -0.08$. (d) is of the normalized Chebyshev coefficients between the first-order damping (\bar{C}_{01}) and third-order damping (\bar{C}_{03}). $\rho(\bar{C}_{01}, \bar{C}_{03}) = 0.05$.

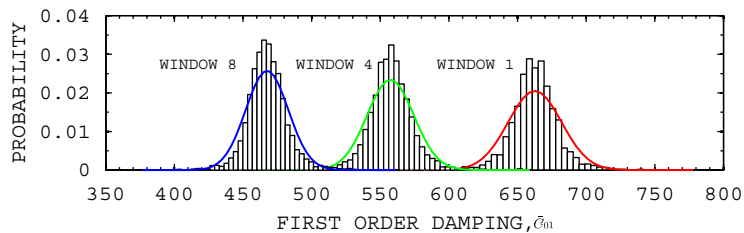


Fig. 9. Histograms and probability density functions (pdf) of the first-order damping normalized Chebyshev coefficient (\bar{C}_{ij}) for different time-history windows. The bin width (or smoothing factor) of the histogram was determined using the normal reference rule (or Scott’s rule). The pdfs were estimated with the assumption of the normal distribution.

uncertainty of the detected changes. Using the Restoring Force Method identification procedure, these objectives can be achieved without knowing the underlying physical characteristics of the identified system.

Using the extracted coefficient distributions, the statistical Hypothesis Test was performed to detect the changes in the distribution means. This test can be performed with the test statistics of two-tailed

T-distribution [20,21]:

$$H_0 : (\mu_1 - \mu_2) = 0, \quad z = \frac{\bar{y}_1 - \bar{y}_2}{\sigma_{(\bar{y}_1 - \bar{y}_2)}} \approx \frac{\bar{y}_1 - \bar{y}_2}{\sqrt{\frac{s_1^2}{n_1} + \frac{s_2^2}{n_2}}}, \quad (7)$$

where H_0 is the null-hypothesis, \bar{y}_1 and \bar{y}_2 are the identified Chebyshev coefficients for two different identification windows, μ_1 and μ_2 are the means of the coefficient distributions from two identification windows, σ_1 and σ_2 are the standard deviations of the coefficient distributions from two identification windows, and s_1 and s_2 the sample standard deviations of the coefficient distributions from two identification windows. In the Hypothesis Tests, the change of the distribution mean was observed with all windows (Windows 1–8) with a 95% confidence level.

5. Bootstrap estimation of identification uncertainty

The uncertainty quantification usually requires many data sets—in Section 4, 3000 data sets were used to measure the identification uncertainty. However, collecting sufficient data sets of large-scale viscous dampers for reliable statistical estimation is very difficult and expensive. Statistical data recycling techniques have been applied successfully in many fields of engineering and science for the error generalization of identification results using insufficient data sets. In this section, the Bootstrap method is used to measure the uncertainty of the damper change detection with a single data set. The Bootstrap estimates of the identification uncertainty with a single data set will be compared with the uncertainty estimates with the multiple data sets discussed in Section 4.

5.1. Overview of the Bootstrap method

The Bootstrap method is a statistical data recycling technique for the uncertainty estimation of any kind of identification parameters. This method is commonly used where the estimation of parameter uncertainty is needed, but an insufficient amount of data is available for a statistically reliable uncertainty quantification. Excellent introductory literature on the Bootstrap method can be found in the work of Efron [22], Efron and Tibshirani [23], Davison and Hinkley [24], and Martinez and Martinez [25].

The Bootstrap method starts with a very simple assumption. An arbitrary parameter (θ) identified using an independently and identically distributed (*i.i.d*) random data set, $\mathbf{y} = (y_1, y_2, \dots, y_n)^T$ with the underlying true distribution (F) can be modeled as

$$\theta = t(F), \quad (8)$$

where $t(\bullet)$ is a nonlinear function of F . Without knowing F , the uncertainty of θ is commonly determined with multiple data sets, $\{\mathbf{y}_1, \mathbf{y}_2, \dots, \mathbf{y}_M\}$, drawn from the same distribution F as

$$s_\theta = \sqrt{\frac{1}{M-1} \sum_{i=1}^M (\theta_i - m_\theta)^2}, \quad (9)$$

where s_θ is the sample standard deviation of θ , m_θ is the sample mean of θ , M is the number of multiple tests, and θ_i is the parameter identified in the i th test.

Instead of performing multiple tests for the uncertainty quantification, the Bootstrap method recycles a single data set, \mathbf{y} with the empirical distribution (\hat{F}). The data recycling is performed with the random selection of a sample (y_k , where $1 \leq k \leq n$) from \mathbf{y} for n times *with replacement*. With replacement, the probability of each sample to be selected is $1/n$. Performing these procedures B times, one can obtain multiple Bootstrap replicates, $\{\mathbf{y}_1^*, \mathbf{y}_2^*, \dots, \mathbf{y}_B^*\}$. The Bootstrap estimate of the parameter uncertainty is determined as

$$s_\theta^* = \sqrt{\frac{1}{B-1} \sum_{i=1}^B (\theta_i^* - m_\theta^*)^2}, \quad (10)$$

where s_θ^* is the Bootstrap standard error of θ , θ_i^* is the parameter identified in the i th Bootstrap replicate of the data set, B is the number of the Bootstrap replicates, and m_θ^* is the Bootstrap estimate of θ defined as

$$m_\theta^* = \frac{1}{B} \sum_{i=1}^B \theta_i^*. \quad (11)$$

In order that $s_\theta \approx s_\theta^*$, the empirical distribution \hat{F} should be close to the true distribution F . Therefore, the following two conditions should be satisfied for the Bootstrap estimation of the standard error:

1. The random data y are *i.i.d.*
2. The empirical distribution \hat{F} is close to the true distribution F .

In the context of the damper identification problem under discussion, however, since the noisy measurement states (\ddot{x}, f) for Damper A and (x, f) for Dampers B and C are time-correlated (i.e., the data are not *i.i.d.*), the standard Bootstrap method described above needs to be modified to deal with the time-dependency. Many modified algorithms have been developed and introduced: model-based resampling [26,27], block resampling [28–30], phase scrambling [31,32], and periodogram resampling [24]. Detailed descriptions of each of these methods can be found in Davison and Hinkley [24], and Hardle et al. [33]. Among these methods, one of the most widely used method is the model-based resampling, because of its simple procedure and good theoretical behavior when the time-series model is correct. Consequently, in this study, the model-based resampling method was employed for the uncertainty estimation of the time-dependent data. In Section 5.2, a detailed Bootstrap-resampling procedure is proposed and described in detail for the cases that the displacement and force were measured (Damper A), and that the acceleration and force were measured (Dampers B and C).

5.2. Bootstrap resampling of noisy response data

Single data sets of Dampers A–C were recycled with the Bootstrap method using the following procedures:

5.2.1. Approach when displacement is measured

A single data set of noisy (5% rms) displacement (x) and force (f) for Dampers B and C was resampled with the Bootstrap method as follows:

1. The same data processing procedures for Dampers B and C in Section 2.2 were performed to obtain the triplet (x, \dot{x}, f) .
2. The Restoring Force Method identification was performed with the noisy (x, \dot{x}, f) . The identification residual (e) was obtained as $e = f - \hat{f}$, where \hat{f} is the identified force using the Restoring Force Method.
3. The auto-regression (AR) was performed for the time histories of x and e . The corresponding AR estimate of x is \hat{x} . The AR orders were determined so as to satisfy the conditions that ε_x and ε_e become *i.i.d.*, where ε_x is the AR residual of x , and ε_e is the AR residual of e . The detailed procedure for determining the optimal AR orders for the ε_x and ε_e is described later in this section.
4. The Bootstrap resampling was performed with the ε_x and ε_e to obtain the Bootstrap replicates of the ε_x and ε_e (ε_x^* and ε_e^* , respectively).
5. The Bootstrap replicates of the displacement (x^*) and force (f^*) were obtained with the sample reconstruction as $x^* = \hat{x} + \varepsilon_x^*$ and $f^* = \hat{f} + \hat{e} + \varepsilon_e^*$.
6. The Bootstrap version of the velocity (\dot{x}^*) was obtained through the differentiation of x^* . In this procedure, the same filter and time-history window as those discussed in Section 2.2 were applied.

A total of 3000 Bootstrap replicates (x^*, \dot{x}^*, f^*) were obtained. The Bootstrap-resampling procedures for Dampers B and C are also illustrated schematically in Fig. 10.

A sample comparison of the original and Bootstrap-resampled data is shown in Fig. 11. The Bootstrap-resampled data show slightly larger dispersion than the original data in the phase plots. The Restoring Force

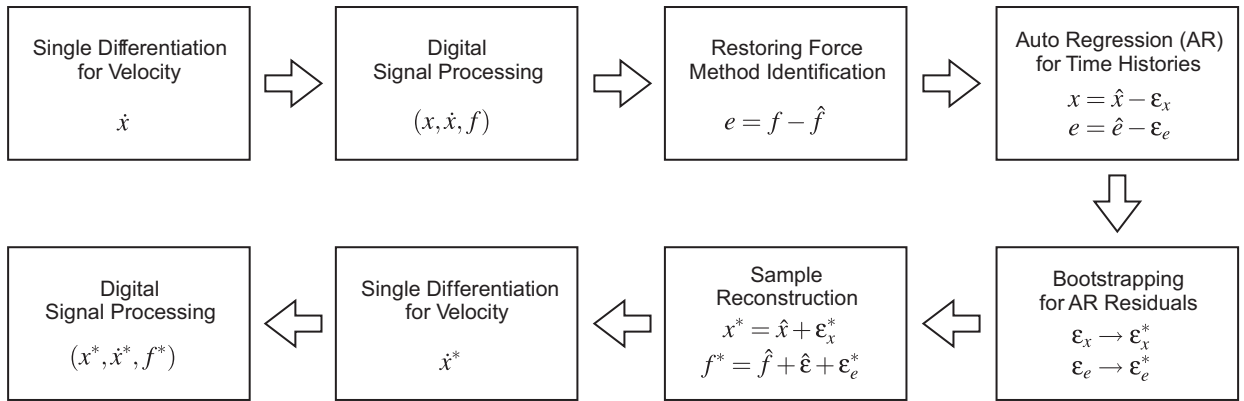


Fig. 10. Bootstrap-resampling procedures for Dampers B and C with measured displacement (x) and force (f).

Method identification was performed with the 3000 Bootstrap replicates, and the corresponding Restoring Force Method coefficients were identified. The Bootstrap standard errors of 3000 identified coefficient sets were estimated using Eq. (10), and compared to the standard deviations of multiple tests. Table 5 shows a comparison of the error estimations of the Restoring Force Method identified coefficients with multiple tests. In the table, the error estimates with the Bootstrap method are larger than those with multiple tests: 7–42% for Damper B and -0.2 –53% for Damper C. Hence, it can be seen that the Bootstrap estimation of the identification error is more conservative than the results obtained through estimation with multiple tests. In addition, the results indicate that the Bootstrap method is applicable to the time-varying system (Damper C), as well as the time-invariant system (Damper B).

5.2.2. Approach when acceleration is measured

Using a single data set of noisy (5% rms) measurements of the acceleration (\ddot{x}) and force (f) for Damper A, the Bootstrap method was applied as follows:

1. The same data processing procedures for Damper A in Section 2.2 were performed to obtain the triplet (x, \dot{x}, f) .
2. The Restoring Force Method identification was performed with the noisy (x, \dot{x}, f) . The identification residual (e) was obtained as $e = f - \hat{f}$, where \hat{f} is the identified force using the Restoring Force Method.
3. The AR was performed for the time histories of \ddot{x} and e . The AR estimate of \ddot{x} is $\hat{\ddot{x}}$. The AR orders of $\hat{\ddot{x}}$ and \hat{e} were determined so as to satisfy the conditions that $\varepsilon_{\ddot{x}}$ and ε_e become *i.i.d.*, where $\varepsilon_{\ddot{x}}$ is the AR residual of $\hat{\ddot{x}}$, and ε_e is the AR residual of e . The detailed procedure for determining the optimal AR orders is described below.
4. The Bootstrap resampling was performed with $\varepsilon_{\ddot{x}}$ and ε_e to obtain the Bootstrap replicates of $\varepsilon_{\ddot{x}}$ and ε_e ($\varepsilon_{\ddot{x}}^*$ and ε_e^* , respectively).
5. The Bootstrap replicates of the acceleration (\ddot{x}^*) and force (f^*) were obtained with the sample reconstruction as $\ddot{x}^* = \hat{\ddot{x}} + \varepsilon_{\ddot{x}}^*$ and $f^* = \hat{f} + \hat{e} + \varepsilon_e^*$.
6. The \ddot{x}^* was integrated and then double-integrated for the Bootstrap version of the velocity (\dot{x}^*) and displacement (x^*), respectively. The same filter and time-history window were applied to \dot{x}^* and x^* as described in Section 2.2.

A total of 3000 Bootstrap replicates (x^*, \dot{x}^*, f^*) were generated. The Bootstrap-resampling procedures for Damper A are also illustrated in Fig. 12.

A sample comparison between the original and Bootstrap-resampled data for Damper A is shown in Fig. 11(a). Unlike Dampers B and C, the range of the Bootstrap-resampled displacement is approximately

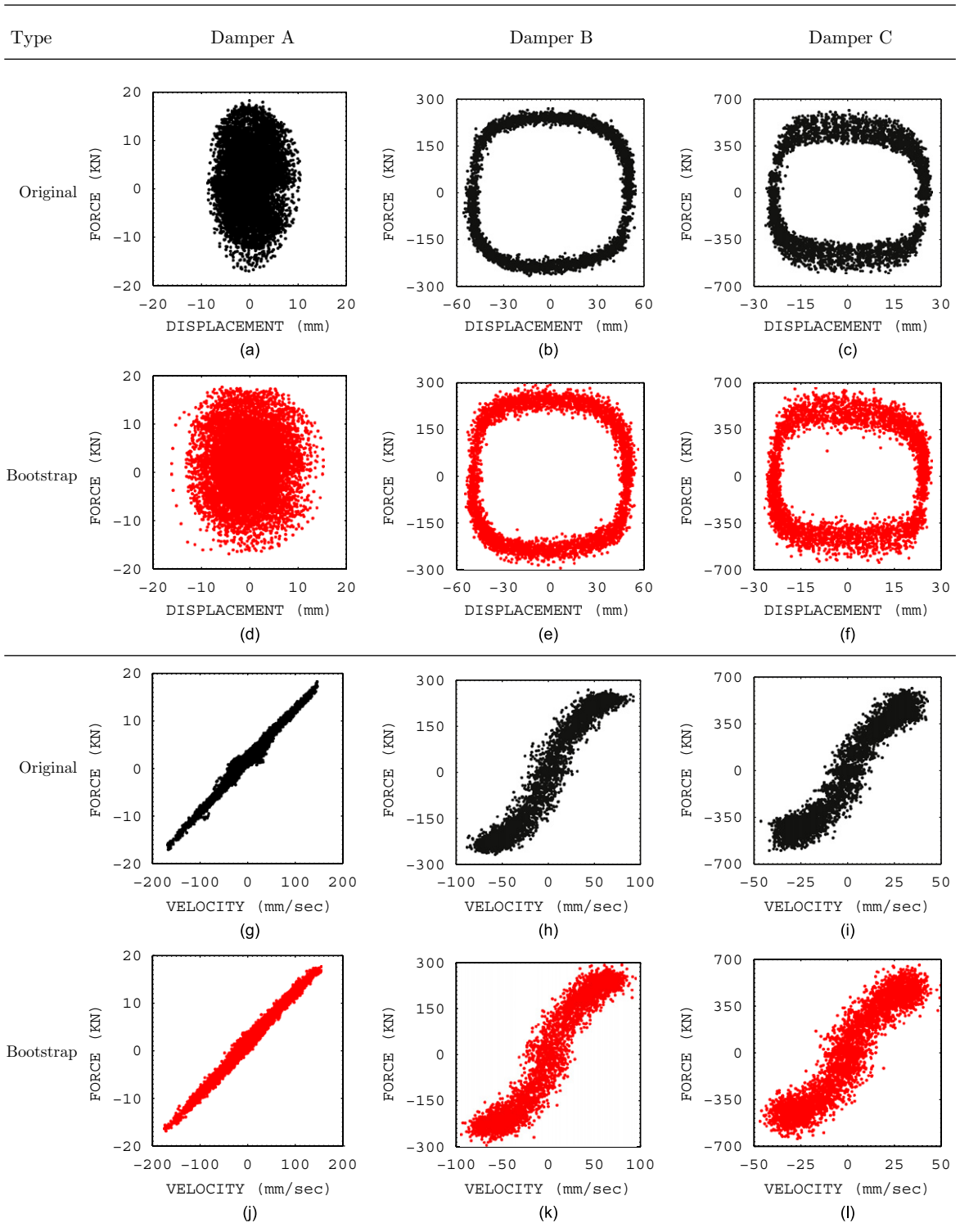


Fig. 11. A comparison of the original and Bootstrap-resampled data for Dampers A, B and C. The upper half of the figure displays displacement–force plots, while the lower half shows the velocity–force plots.

Table 5
Bootstrap estimations of standard errors for the coefficients identified using the Restoring Force Method.

Type	Damper A			Damper B			Damper C		
	Multiple	Bootstrap	Ratio	Multiple	Bootstrap	Ratio	Multiple	Bootstrap	Ratio
\tilde{C}_{10}	0.19	0.32	1.68	14.26	17.35	1.22	32.17	42.14	1.31
\tilde{C}_{01}	0.16	0.31	1.94	8.60	12.22	1.42	17.17	26.21	1.53
\tilde{C}_{30}	0.14	0.32	2.29	14.09	18.63	1.32	28.40	37.81	1.33
\tilde{C}_{03}	0.10	0.20	2.00	9.14	12.49	1.37	20.71	27.47	1.33
\tilde{a}_{10}	0.69	1.44	2.09	115.28	149.10	1.29	245.46	311.77	1.27
\tilde{a}_{01}	0.74	1.64	2.22	86.03	104.55	1.22	198.68	235.09	1.18
\tilde{a}_{30}	2.32	4.76	2.05	360.35	474.97	1.32	786.05	983.70	1.25
\tilde{a}_{03}	2.26	5.67	2.48	322.88	395.84	1.23	669.23	823.17	1.23
a_{10}	6.27E-2	7.13E-2	1.14	2.09	2.67	1.28	7.85	11.60	1.48
a_{01}	5.56E-3	1.01E-2	1.82	0.90	1.06	1.18	3.63	4.58	1.26
a_{30}	2.36E-3	7.03E-4	0.30	2.12E-3	2.71E-3	1.28	4.24E-2	5.14E-2	1.21
a_{03}	6.69E-7	1.30E-6	1.94	4.35E-4	4.66E-4	1.07	8.32E-3	8.13E-3	0.98
NMSE (%)	7.90E-3	2.05E-2	2.59	2.54E-2	3.02E-2	1.19	2.98E-2	2.98E-2	1.00

The Bootstrap estimates are compared with the standard deviations through the multiple tests shown in Table 4. The sample size is 3000 for both the Bootstrap and multiple test estimates.

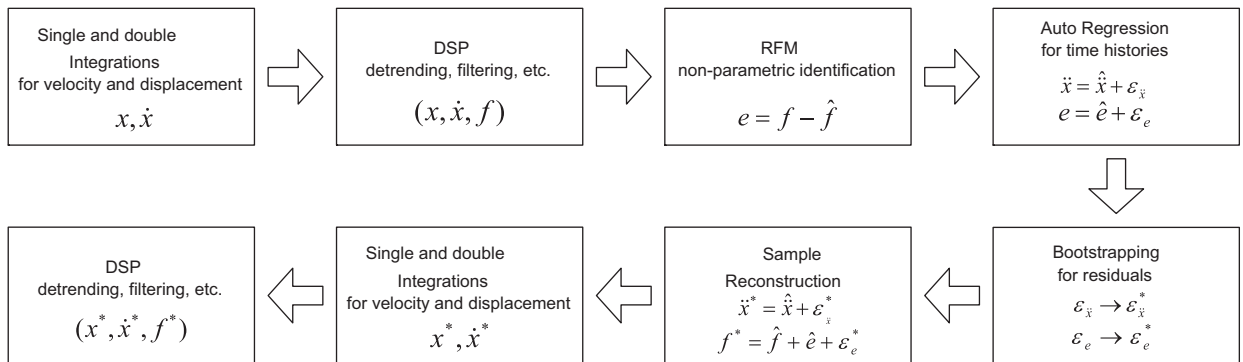


Fig. 12. Bootstrap-resampling procedures for Damper A with measured acceleration (\ddot{x}) and force (r).

twice larger than that of the original displacement in the displacement–force plot, while the velocity–force plots of two data sets are almost identical.

5.2.3. Issues involving the AR procedure

The above results indicate that using the measured acceleration, the Bootstrapping for the velocity through single-integration was successful, but the Bootstrapping for the displacement through double-integration failed. In the model-based Bootstrap method, the resampling results are largely dependent on the performance of the AR identification. The AR is performed to remove the trends of the time-series data, and with successful AR, the corresponding AR residuals ($\epsilon_{\dot{x}}$ and ϵ_e for Damper A, and ϵ_x and ϵ_e for Dampers B and C) become *i.i.d.* Fig. 13 shows the significance of the time-correlation for different AR orders. The significance of the time-correlation is commonly measured with the correlation coefficient (ρ) in a lag plot. Here, the lag is defined as a fixed time distance. For example, for the vector $\epsilon_e = \{\epsilon_{e_1}, \epsilon_{e_2}, \dots, \epsilon_{e_n}\}$ for Damper B, the ϵ_{e_2} and ϵ_{e_5} have a lag with order *three*. Hence, in the lag plot (usually with order one), which has the x -axis of ϵ_{e_i} and the

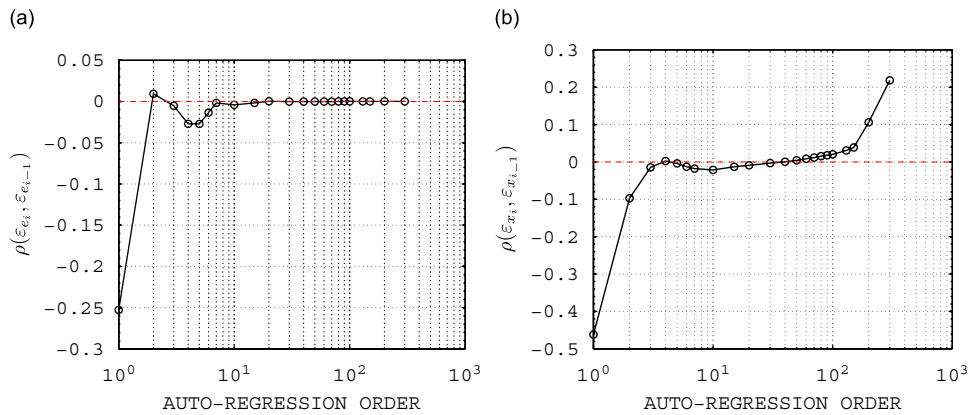


Fig. 13. Measured first-order time-correlations for different auto-regression (AR) orders. (a) The AR residual of the identified restoring force (ε_e). (b) The displacement (ε_x). The time-correlations were measured with the correlation coefficients of the order-one lags for ε_e and ε_x . The definition of the order-one lags is explained in the text.

y-axis of $\varepsilon_{e_{i-1}}$ ($i = 2, 3, \dots, n$), the correlation coefficient $\rho(\varepsilon_{e_i}, \varepsilon_{e_{i-1}})$ measures the serial correlations of the ε_e in time. In Fig. 13(a), the $\rho(\varepsilon_{e_i}, \varepsilon_{e_{i-1}})$ asymptotically approaches to zero as the AR order increases. However, Fig. 13(b) illustrates that the $\rho(\varepsilon_{x_i}, \varepsilon_{x_{i-1}})$ approaches to zero as the AR order approaches from 1 to 40. Then, the $\rho(\varepsilon_{x_i}, \varepsilon_{x_{i-1}})$ increases as the AR order increases more than 40. This result indicates that the AR for the identification residual (e) becomes overfitted when the AR order is greater than 40. Consequently, the AR order of 40 was used in the Bootstrap resampling for Damper B. The same procedure of determining the optimal AR order was applied for Dampers A and C.

Although the serial correlations in time were carefully removed with the optimal AR orders, however, perfect removal of the time correlations is almost impossible. Consequently, a slight amount of time-correlation will affect the results of differentiation or integration. In this study, the results indicate that the unremoved trend does not significantly affect to the results of the single differentiation ($x^* \rightarrow \dot{x}^*$) and integration ($\dot{x}^* \rightarrow x^*$). However, the unremoved trend significantly influences the results of the second integration ($\dot{x}^* \rightarrow x^*$) as the example of Damper A. Consequently, the Bootstrapping for the displacement becomes unsuccessful. Therefore, in the application of the Bootstrap method to noisy measurements, it is recommended that the force as well as the displacement of the damper be directly measured.

6. Summary and conclusion

Experimental and analytical studies were conducted to develop probabilistic change detection methodology for *in situ* monitoring of nonlinear viscous dampers with measurement uncertainty. A unique data set was assembled from a collection of carefully conducted experimental studies of heavily instrumented, full-scale, nonlinear viscous dampers, spanning a broad range of sizes that are commonly used in civil infrastructure applications. Due to their inherent power in dealing with complex nonlinear phenomena, such as those encountered at various scales in the investigated nonlinear dampers, model-free identification techniques utilizing non-parametric system identification approaches were used to analyze the available measurements.

It was found that the coefficients identified using the Restoring Force Method can be used as excellent indicators (or features) (1) to detect the changes of nonlinear systems, (2) to interpret the physical meaning of the detected changes, and (3) to quantify the uncertainty of the detected system changes.

The Bootstrap method was also investigated for uncertainty quantification of the detected changes when the measurement data are insufficient for reliable statistical inference. Using the Bootstrap method, the uncertainty of the identification was estimated reasonably accurately, even with a single data set, when the displacement and force were measured.

Acknowledgments

This study was supported in part by grants from the National Science Foundation (NSF), the National Aeronautics and Space Administration (NASA), and the California Department of Transportation (Caltrans).

The assistance of N. Makris and C. Black in the experimental tests at the University of California, Berkeley is appreciated.

References

- [1] T.T. Soong, M.C. Constantinou, *Passive and Active Structural Vibration Control in Civil Engineering (CISM International Centre for Mechanical Sciences)*, first ed., Springer, New York, 1994.
- [2] T.T. Soong, G.F. Dargush, *Passive Energy Dissipation Systems in Structural Engineering*, Wiley, New York, 1997.
- [3] HITEC, Guidelines for the testing of seismic isolation and energy dissipating devices, Civil Engineering Research Foundation Report: HITEC 96-02. Highway Innovative Technology Evaluation Center, 1996.
- [4] HITEC, Evaluation findings for Enidine, Inc. viscous damper, Civil Engineering Research Foundation Report: HITEC 99-03 Highway Innovative Technology Evaluation Center, 1999.
- [5] HITEC, Evaluation findings for Taylor devices fluid viscous damper, Civil Engineering Research Foundation Report: HITEC 99-02, Highway Innovative Technology Evaluation Center, 1999.
- [6] HITEC, Summary of evaluation findings for the testing of seismic isolation and energy dissipating devices. Civil Engineering Research Foundation Report No. 40404. Highway Innovative Technology Evaluation Center, 1999.
- [7] H.-B. Yun, F. Tasbihgoo, S.F. Masri, J.P. Caffrey, R.W. Wolfe, N. Makris, C. Black, Comparison of modeling approaches for full-scale nonlinear viscous dampers, *Journal of Vibration and Control* 14 (1–2) (2008) 51–76.
- [8] H.-B. Yun, S.F. Masri, Stochastic change detection in uncertain nonlinear systems using reduced-order models: system identification, *Journal of Smart Materials and Structures* 17 (2008) 1–13.
- [9] H.-B. Yun, R.D. Nayeri, F. Tasbihgoo, M. Wahbeh, J.P. Caffrey, R. Wolfe, R. Nigbor, S.F. Masri, A.M. Abdel-Ghaffar, L.-H. Sheng, Monitoring the collision of a cargo ship with the Vincent Thomas bridge, *Structural Control and Health Monitoring* 15 (2) (2007) 183–206.
- [10] J.P. Den Hartog, *Mechanical Vibrations*, McGraw-Hill, New York, 1956.
- [11] N. Makris, M.C. Constantinou, Fractional derivative model for viscous dampers, *Journal of Structural Engineering, ASCE* 117 (1991) 2708–2724.
- [12] N. Makris, M.C. Constantinou, G.F. Dargush, Analytical model of viscoelastic fluid dampers, *Journal of Structural Engineering, ASCE* 119 (11) (1993) 3310–3325.
- [13] M.C. Constantinou, M.D. Symans, P. Tsopelas, D.P. Taylor, Fluid viscous dampers in applications of seismic energy dissipation and seismic isolation, *ATC-17-1 Seminar on Seismic Isolation, Passive Energy Dissipation, and Active Control*, Vol. 2, San Francisco, CA, USA, March 1993, pp. 581–592.
- [14] M.C. Constantinou, M.D. Symans, Experimental study of seismic response of buildings with supplemental fluid dampers, *Structural Design of Tall Buildings* 2 (1993) 93–132.
- [15] S.F. Masri, T.K. Caughey, A nonparametric identification technique for nonlinear dynamic problems, *Journal of Applied Mechanics Transactions on ASME* 46 (2) (1979) 433–447.
- [16] J.C. Mason, D.C. Handscomb, *Chebyshev Polynomials*, CRC Press, Boca Ration, FL, USA, 2003.
- [17] K. Worden, G.R. Tomlinson, *Nonlinearity in Structural Dynamics: Detection Identification and Modelling*, Institute of Physics Publications, Bristol and Philadelphia, 2001.
- [18] D.W. Scott, On optimal and data-based histograms, *Biometrika* 66 (3) (1979) 605–610.
- [19] D.W. Scott, *Multivariate Density Estimation: Theory, Practice and Visualization*, Wiley, New York, 1992.
- [20] W. Mendenhall, T. Sincich, *Statistics for Engineering and the Sciences*, fourth ed., Prentice-Hall, New York, 1995.
- [21] R.V. Hogg, E.A. Tanis, *Probability and Statistical Inference*, fifth ed., Prentice Hall, New York, 1997.
- [22] B. Efron, Bootstrap methods: another look at the jackknife, *Annals of Statistics* 7 (1979) 1–26.
- [23] B. Efron, R.J. Tibshirani, *An Introduction to the Bootstrap*, CRC Press LLC, Boca Raton, FL, USA, 1993.
- [24] A.C. Davison, D.V. Hinkley, *Bootstrap Methods and their Application*, Cambridge University Press, New York, 1997.
- [25] W.L. Martinez, A.R. Martinez, *Computational Statistics Handbook with MATLAB*, CRC Press LLC, Boca Raton, FL, USA, 2002.
- [26] B. Efron, R.J. Tibshirani, Bootstrap methods for standard errors, confidence intervals, and other measures of statistical accuracy, *Statistical Science* 1 (1986) 54–77.
- [27] J.-P. Kreiss, J. Franke, Bootstrapping stationary autoregressive moving average models, *Journal of Time Series Analysis* 13 (1992) 297–317.
- [28] P. Hall, Resampling a coverage pattern, *Stochastic Processes and their Applications* 20 (1985) 231–246.
- [29] E. Carlstein, The use of subsamples values for estimating the variance of general statistic from a stationary sequence, *Annals of Statistics* 14 (1986) 1171–1194.
- [30] S.G. Shi, Local bootstrap, *Annals of the Institute of Statistical Mathematics* 43 (1991) 667–676.

- [31] J. Theiler, S. Eubank, A. Longtin, B. Galdrikian, J.D. Farmer, Testing for nonlinearity in time series: the method of surrogate data, *Physical Review D* 58 (1992) 77–94.
- [32] J. Timmer, Power of surrogate data testing with respect to non-stationarity, *Physical Review E* 58 (1998) 5153–5156.
- [33] W. Härdle, J. Horowitz, J.-P. Kreiss, Bootstrap methods for time series, *International Statistical Review* 71 (2) (2003) 435–459.